Energy efficient cornering using over-actuation

Downloaded from: https://research.chalmers.se, 2026-11-12 01:57 UTC

Citation for the original published paper (version of record):
Edrén, J., Jonasson, M., Jerrelind, J. et al (2019). Energy efficient cornering using over-actuation. Mechatronics, 59: 69-81

N.B. When citing this work, cite the original published paper.

research.chalmers.se offers the possibility of retrieving research publications produced at Chalmers University of Technology. It covers all kind of research output: articles, dissertations, conference papers, reports etc. since 2004. research.chalmers.se is administrated and maintained by Chalmers Library

(article starts on next page)

Energy efficient cornering using over-actuation

Johannes Edrén[1]*, Mats Jonasson[2,1], Jenny Jerrelind[1], Annika Stensson Trigell[1] and Lars Drugge[1]
[1] KTH Vehicle Dynamics, Department of Aeronautical and Vehicle Engineering, KTH Royal Institute of Technology, Stockholm, Sweden and SHC (Swedish Hybrid Vehicle Centre)
[2] Active Safety, Volvo Car Corporation, Gothenburg, Sweden

Teknikringen 8
SE-100 44 Stockholm, Sweden

E-mail: edren@kth.se

This work deals with utilisation of active steering and propulsion on individual wheels in order to improve a vehicle's energy efficiency during a double lane change manoeuvre at moderate speeds. Through numerical optimisation, solutions have been found for how wheel steering angles and propulsion torques should be used in order to minimise the energy consumed by the vehicle travelling through the manoeuvre. The results show that, for the studied vehicle, the energy consumption due to cornering resistance can be reduced by approximately 10 % compared to a standard vehicle configuration. Based on the optimisation study, simplified algorithms to control wheel steering angles and propulsion torques that results in more energy efficient cornering are proposed. These algorithms are evaluated in a simulation study that includes a path tracking driver model. Based on a combined rear axle steering and torque vectoring control an improvement of 6-8 % of the energy consumption due to cornering was found. The results indicate that in order to improve energy efficiency for a vehicle driving in a non-safety-critical cornering situation the force distribution should be shifted towards the front wheels.

Keywords: Vehicle control, Energy efficiency, Over-actuation, Optimisation.

1. INTRODUCTION

In addition to vehicle performance and safety, the overall energy efficiency is also important. With traditional vehicle configurations the distribution of wheel steering angles and propulsion torques are limited by the mechanical drive train and suspension systems. With electrified drive trains, the ability to implement individual control of wheel steering angles and propulsion is an option. Individual control of the wheels opens up further potential to make the vehicle more energy efficient, both during straight-line driving and cornering. In this work, optimisation is used as a method to find strategies to control a vehicle during mild cornering manoeuvring in order to minimise the energy consumed. Mild cornering situations are chosen since that is more frequent during highway driving than severe at-the-limit situations and would therefore contribute more to the total energy consumption.

In [1] it is recognised that optimal torque distribution can improve energy efficiency and in [2] energy efficient control allocation is implemented to control wheel torques in order to make the vehicle to follow given vehicle velocities. This is done by also incorporating the efficiency of the individual wheel motors. In [3] the approach is further expanded to allow for different wheel motor efficiencies, resulting in that more torque is distributed toward the motors with highest energy efficiency. In [4], online control of the energy dissipation rate of tyres has also been studied, where the dissipated energy of the sliding part of the tyres has been calculated to control wheel torques and steering angles to minimise the total energy dissipation rate for each moment in time. In that work, the motion of the chassis is given by the same reference model, meaning that the energy consumed when exciting the vehicle motion does not contribute to the estimated energy loss. Yaw motion in particular is requested to be at the same level as that chosen reference model. In [5] energy efficient torque vectoring has been studied, but not compared to other vehicle configuration types. In [6] different vehicle configuration types has been evaluated for optimizing the ability to follow a path, but not minimizing the energy. The goal in this work is to extend the scope in order to find energy-efficient strategies to move a vehicle between two points in space, with more freedom as regards how the vehicle motion can be controlled, compared to the work in [4].

A brief outline of the paper follows below. The vehicle model is presented in Chapter 2. The optimisation study is introduced in Chapter 3 and the results from the optimisation study are presented in Chapter 4. Chapter 5 describes the simulation study and the implemented control algorithms such as torque vectoring control (TVC) and control of rear axle steering (RAS). The results from the simulations are presented in Chapter 6. The conclusions from the study are described in Chapter 7.

2. VEHICLE MODEL

The vehicle chosen to be studied in this work is a typical passenger car of the sports utility vehicle (SUV) type. This model is based on [7] and has 6 degrees of freedom, representing the vehicle body's motion, as shown in Figure 1. The motion resistances due to rolling friction and aerodynamic drag are ignored in the model. This is because energy losses from these forces are more or less constant in this case, where driving distance and vehicle speed are assumed to be constant. Instead the motion resistance energy is calculated separately and added to the final energy consumption. The vehicle motion is guided by springs, dampers and anti-roll bars, and in addition to [7] the suspension kinematic effects are represented by the roll and pitch axis heights.

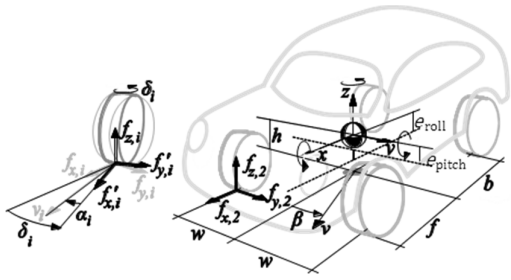

Figure 1. Vehicle model and coordinate system definition $i \in \{1,2,3,4\} = \{FL, FR, RL, RR\}$.

A Pacejka tyre model for pure lateral slip conditions is implemented [8]. It is assumed that the tyres can be modelled by using the longitudinal force as input directly, with the wheel spin being neglected. The tyre force limitations are due to the vertical load $f_{z,i}$, the tyre-road friction coefficient μ and the vertical load sensitivity $f_{x,y,i}^{max}$. The vertical load sensitivity is modelled as:

$$f_{x,y,i}^{max} = \left(\mu \cdot f_{z,i} \cdot \left(p_{d1} - p_{d2}\Delta f_{z,i}\right)\right), \tag{1}$$

where p_{d1} and p_{d2} are the tyre load sensitivity factors. The load sensitivity has a substantial impact on how the load transfer will affect the maximum force that can be utilised by the tyres. $\Delta f_{z,i}$ is the load difference from the static load f_z^{nom} and is assumed to be given by:

$$\Delta f_{z,i} = \frac{f_{z,i} - f_z^{nom}}{f_z^{nom}}. \tag{2}$$

To account for the presence of longitudinal tyre forces, the lateral tyre force calculation is modelled with an elliptical combined slip model giving the lateral force, $f_{y,i}$:

$$f_{y,i} = \sin\left(C_i \arctan(B_i \alpha_i)\right) \cdot \sqrt{\left(f_{x,y,i}^{max}\right)^2 - \left(f_{x,i}\right)^2}, \tag{3}$$

in which $f_{x,i}$ is the longitudinal tyre force, α_i is the tyre slip angle, while B_i and C_i are the Magic Formula (MF) shape factors [7]. The relaxation dynamics dependent on the tyre slip angle $\dot{\alpha}_i$ and the first-order speed are given by:

$$\dot{\alpha}_i = \frac{v_{x,i}}{L_i}\left(\frac{v_{y,i}}{v_{x,i}} - \alpha_i - \delta_i\right), \tag{4}$$

where L_i is the relaxation length, δ_i is the steering angle, and $v_{x,i}$ and $v_{y,i}$ are the longitudinal and lateral speeds of the wheel corner, respectively. The wheel forces will act upon the vehicle, giving the total vehicle forces F_x, F_y and F_z, which are the total longitudinal, lateral and vertical forces on the vehicle:

$$\begin{aligned} F_x = {} & f_{x,1}\cos(\delta_1) + f_{x,2}\cos(\delta_2) + f_{x,3}\cos(\delta_3) + f_{x,4}\cos(\delta_4) \\ & - f_{y,1}\sin(\delta_1) - f_{y,2}\sin(\delta_2) - f_{y,3}\sin(\delta_3) - f_{y,4}\sin(\delta_4), \end{aligned} \tag{5}$$

$$\begin{aligned} F_y = {} & f_{y,1}\cos(\delta_1) + f_{y,2}\cos(\delta_2) + f_{y,3}\cos(\delta_3) + f_{y,4}\cos(\delta_4) \\ & + f_{x,1}\sin(\delta) + f_{x,2}\sin(\delta_2) + f_{x,3}\sin(\delta_3) + f_{x,4}\sin(\delta_4) \end{aligned} \tag{6}$$

and

$$F_z = f_{z,1} + f_{z,2} + f_{z,3} + f_{z,4}. \tag{7}$$

The total vehicle roll, pitch and yaw torques, M_x, M_y and M_z, are derived according to Equations 8 to 11. The contribution of jacking forces and anti-dive/anti-pitch is modelled by the centre of gravity (CoG) height, h, over the respective axes e_{roll}, e_{pitch}. f, b and w are the distances from the vehicle CoG to the wheels (see Figure 1):

$$M_x = \left(f_{z,1} - f_{z,2} + f_{z,3} - f_{z,4}\right)w + F_y(h - e_{roll}) \tag{8}$$

$$M_y = -\left(f_{z,1} + f_{z,2}\right)f + \left(f_{z,3} + f_{z,4}\right)b - F_x\left(h - e_{pitch}\right) \tag{9}$$

$$\begin{aligned} M_z = &-w \cdot f_{x,1}\cos(\delta_1) + w \cdot f_{x,2}\cos(\delta_2) - w \cdot f_{x,3}\cos(\delta_3) + w \cdot f_{x,4}\cos(\delta_4) \\ &+f \cdot f_{x,1}\sin(\delta_1) + f \cdot f_{x,2}\sin(\delta_2) - \mathrm{b} \cdot f_{x,3}\sin(\delta_3) - \mathrm{b} \cdot f_{x,4}\sin(\delta_4) \\ &+f \cdot f_{y,1}\cos(\delta_1) + f \cdot f_{y,2}\cos(\delta_2) - b \cdot f_{y,3}\cos(\delta_3) - b \cdot f_{y,4}\cos(\delta_4) \\ &+w \cdot f_{y,1}\sin(\delta_1) - w \cdot f_{y,2}\sin(\delta_2) + w \cdot f_{y,3}\sin(\delta_3) - w \cdot f_{y,4}\sin(\delta_4), \end{aligned} \tag{10}$$

The suspension kinematic effects during roll and pitch are modelled by the introduction of roll and pitch axes. The vertical forces are given by the vehicle states of vertical position z, pitch angle θ and roll angle φ. The springs are characterised by their stiffness, k_i, the anti-roll bars by k_{12}, k_{34}, the dampers by the damping coefficient d_i and m is the vehicle mass.

$$\begin{aligned} f_{z,1} = &\frac{1}{2(f+b)}\left(b\left(mg - F_y\frac{h - e_{roll}}{w}\right) - F_x\left(h - e_{pitch}\right)\right) \\ &-k_1(z + z_{A1} - f\theta + w\varphi) - k_{12}2w\varphi - d_1\left(\dot{z} - f\dot{\theta} + w\dot{\varphi}\right), \end{aligned} \tag{11}$$

$$\begin{aligned} f_{z,2} = &\frac{1}{2(f+b)}\left(b\left(mg + F_y\frac{h - e_{roll}}{w}\right) - F_x\left(h - e_{pitch}\right)\right) \\ &-k_2(z + z_{A2} - f\theta - w\varphi) + k_{12}2w\varphi - d_2\left(\dot{z} - f\dot{\theta} - w\dot{\varphi}\right), \end{aligned} \tag{12}$$

$$\begin{aligned} f_{z,3} = &\frac{1}{2(f+b)}\left(f\left(mg - F_y\frac{h - e_{roll}}{w}\right) + F_x\left(h - e_{pitch}\right)\right) \\ &-k_3(z + z_{A3} + b\theta + w\varphi) - k_{34}2w\varphi - d_3\left(\dot{z} + b\dot{\theta} + w\dot{\varphi}\right), \end{aligned} \tag{13}$$

$$\begin{aligned} f_{z,4} = &\frac{1}{2(f+b)}\left(f\left(mg + F_y\frac{h - e_{roll}}{w}\right) + F_x\left(h - e_{pitch}\right)\right) \\ &-k_4(z + z_{A4} + b\theta - w\varphi) + k_{34}2w\varphi - d_4\left(\dot{z} + f\dot{\theta} - w\dot{\varphi}\right) \end{aligned} \tag{14}$$

Assuming planar motion, with longitudinal acceleration $a_x$and lateral acceleration a_y, and vertical acceleration a_z, the equations of motion guiding the translational vehicle body are described by:

$$\left(a_x + \ddot{\theta}\left(e_{pitch} + z\right)\right)m = F_x, \tag{15}$$

$$\left(a_y - \ddot{\varphi}(e_{roll} + z)\right)m = F_y, \tag{16}$$

and

$$(a_z + g)m = F_z. \tag{17}$$

The vehicle chassis' angular dynamics including body yaw angle ψ, are described by:

$$\ddot{\varphi}I_{xx} - ma_y\left(e_{pitch} + z\right) + (a_z + g)m\left(e_{pitch} + z\right)\sin(\varphi) = M_x, \tag{18}$$

$$\ddot{\theta}I_{yy} + ma_x(e_{roll} + z) + (a_z + g)m(e_{roll} + z)\sin(\theta) = M_y, \tag{19}$$

$$\ddot{\psi}I_{zz} = M_z, \tag{20}$$

$$a_y = \dot{v_y} + v_x\dot{\psi}, \tag{21}$$

$$a_x = \dot{v_x} - v_y\dot{\psi}. \tag{22}$$

The parameters for the vehicle model used for optimisation are presented in Table 1.

Table 1. Vehicle parameters for the studied vehicle model.

Parameter	Symbol	Value
Vehicle mass	m	2353 kg
Vehicle roll moment of inertia	I_{xx}	850 kgm^2
Vehicle pitch moment of inertia	I_{yy}	4500 kgm^2
Vehicle yaw moment of inertia	I_{zz}	4561 kgm^2
CoG-to-front-axle distance	f	1.371 m
CoG-to-rear-axle distance	b	1.486 m
Half track width	w	0.81 m
CoG-to-ground height	h	0.66 m
CoG-to-roll-axis distance	e_{roll}	0.51 m
CoG-to-pitch-axis distance	e_{pitch}	0.35 m
Front spring stiffness	k_1, k_2	41400 N/m
Rear spring stiffness	k_3, k_4	44800 N/m
Front anti-roll-bar stiffness	k_{12}	12883 N/m
Rear anti-roll-bar stiffness	k_{34}	6086 N/m
Front damper coefficient	d_1, d_2	2000 Ns/m
Rear damper coefficient	d_3, d_4	3500 Ns/m
Front MF tyre stiffness	B_1, B_2	19.2
Rear MF tyre stiffness	B_3, B_4	21.3
MF tyre shape factor	C_i	1
Tyre relaxation length	L_i	0.15 m
Tyre load sensitivity factors	p_{d1}, p_{d2}	1.02, 0.09
Tyre nominal load	f_z^{nom}	4100 N

To be able to study the difference in how the vehicle utilises the vertical loads in order to produce friction, the friction utilisation, η_i, is calculated according to:

$$\eta_i = \sqrt{\frac{{f_{x,i}}^2 + {f_{y,i}}^2}{{f_{z,i}}^2}}. \tag{23}$$

3. THE STUDIED MANOEUVRE

The manoeuvre chosen is the Consumers Union double-lane change [9]. The test was performed by driving the vehicle through a vehicle lane marked by a number of cones, positioned at global coordinates as illustrated in Figure 2. The vehicle's entry and exit speeds are fixed at 12 m/s, which results in a maximum lateral acceleration of about 0.5 g. This is to mimic a realistic driving scenario that is far from limit conditions. The bound around the second and third cone pair are a polynomial functions that describe how close to the cone the vehicle is allowed. The shape of this forbidden region is described in Chapter 4.

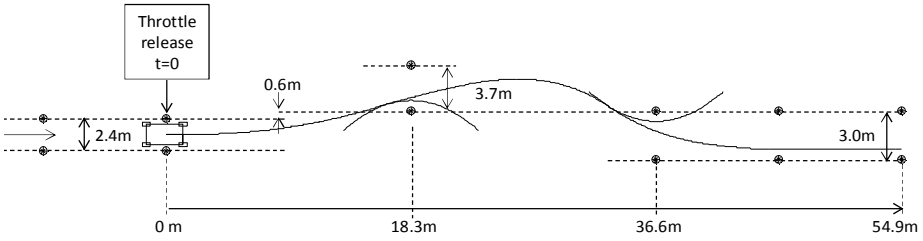

Figure 2. Definition of the manoeuvre used in the optimisation study and the forbidden regions.

4. OPTIMISATION STUDY SETUP

4.1 Actuators

Six different vehicle configurations are chosen to be studied, see Table 2. These include front axle steering (FAS) and rear axle steering (RAS) with the right and left wheel of each axle steered at the same angle, and RAS having a smaller maximum steering angle, to represent a rear wheel steered implementation that is possible in today's vehicles. All-wheel steering (AWS) has full individual steering of each wheel. Propulsion forces are studied in two variants. The first is four-wheel drive with equal distribution between front and rear axle (4WD) and finally full individual drive (i-AWD). Assumed actuator constraints are described in Table 3.

Table 2. Studied vehicle configurations.

Vehicle	FAS	RAS	AWS	4WD	i-AWD
A	■			■	
B	■				■
C	■	■		■	
D	■	■			■
E			■	■	
F			■		■

Table 3. Actuator constraints used in the optimisation study.

Actuator system	Constraints
FAS	$-22.9° < \delta_{front} < 22.9°, -75°/s < \delta_{front}/\mathrm{dt} < 75°/s$
RAS	$-2.9° < \delta_{rear} < 2.9°, -20°/s < \delta_{rear}/\mathrm{dt} < 20°/s$
AWS	$-22.9° < \delta_i < 22.9°, -75°/s < \delta_i/dt < 75°/s, i = 1,2,3,4$
4WD	$0 < T < 300\ \mathrm{Nm}, -150\ \mathrm{kNm/s} < dT/dt < 150\ \mathrm{kNm/s}$
i-AWD	$0 < T_i < 300\ \mathrm{Nm}, -150\ \mathrm{kNm/s} < dT_i/dt < 150\ \mathrm{kNm/s}, i = 1,2,3,4$

4.2 Optimisation procedure

To study how much the vehicle's energy efficiency can be affected by individual control of steering and propulsion, optimisation was used. The chosen optimisation tool, Optimica, is written in the Modelica language [10-11]. Optimica is an open-source software from JModelica.org [12]. Figure 3 shows the flow of the procedure needed for the optimisation problem formulation.

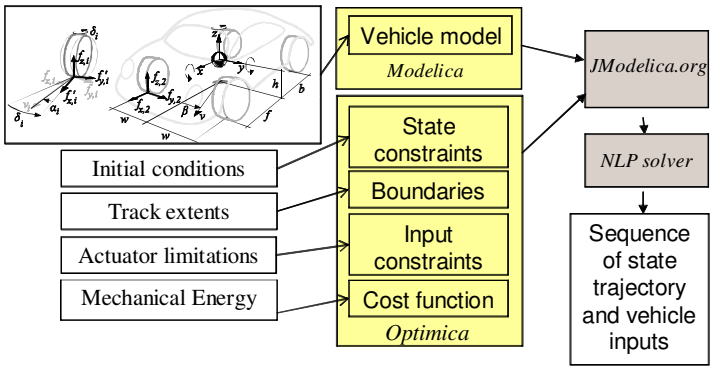

Figure 3. Optimisation problem formulation procedure [10].

The optimisation was initialised when the centre of gravity (CoG) of the vehicle was in the position marked 'throttle release' in Figure 2. At this position, the vehicle was centred between the cone pairs and was directed with zero yaw-angle, zero yaw-rate and zero lateral velocity.

For the test manoeuvre, cones were used to mark the permitted regions. Each cone j marked the edge of a forbidden region expressed as:

$$Y \geq Y_{cone,j} + \left(k\left(X - X_{cone.j}\right)\right)^2, \tag{24}$$

where X and Y are the coordinates for the forbidden region associated with the j:th cone positioned at $X_{cone.j}$, $Y_{cone,j}$ (the cone coordinates), and k is the shape factor of the polynomial. $k = 0.3$ was chosen for this study since it gave a reasonable path. The right-hand row of cones at the final stage of the manoeuvre is treated as a boundary

condition for the vehicle's lateral position Y.

$$Y \geq -1.11 \text{ m} \tag{25}$$

The whole family of cones determines the total region not to be violated. Due to rear axle steering being utilised in some of the vehicle configurations, the solution can begin to separate yaw dynamics and lateral motion. The constraints of the chassis are therefore modified to ensure that both the front and rear axle will manage the cone track, see Figure 4. This results in the optimal solution trying to keep the heading of the vehicle, and unrealistic values of body slip are thereby inhibited. In Table 4, the boundary conditions set for the vehicle running through the manoeuvre are listed.

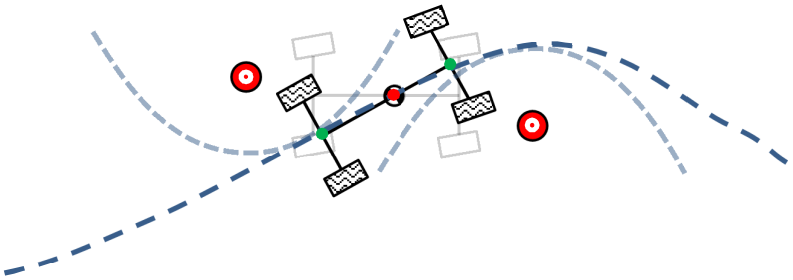

Figure 4. Forbidden region around cones for the centre of gravity for front and rear axles.

Table 4. Chosen initial and final conditions for the manoeuvre.

Position	Attitude	Velocities
$X_0 = 0$ m	$\psi_o = 0$ rad	$\dot{x}_o = v_{x\,init}$ m/s
$Y_0 = 0$ m	$\theta_o = 0$ rad	$\dot{x}_f = v_{x\,init}$ m/s
$Z_o = 0$ m	$\varphi_o = 0$ rad	$\dot{y}_o = 0$ m/s
$X_f = 54.9$ m		$\dot{z}_o = 0$ m/s
		$\dot{\theta}_o = 0$ rad/s
		$\dot{\varphi}_o = 0$ rad/s
		$\dot{\varphi}_f = 0$ rad/s

4.3 Optimisation problem formulation

The control signals that will result in the best solution for the vehicle to accomplish the manoeuvre are found by optimisation (Figure 4). The cost function yields a solution that aims to minimise the mechanical energy consumed during the manoeuvre. Because the vehicle drag forces are neglected, the dominant force left to slow down the vehicle is the cornering resistance. For each wheel, the longitudinal force $f_{x,i}$ multiplied by the longitudinal speed $v_{xw,i}$ is calculated into a mechanical power P_i for each time step,

$$P_i = v_{xw,i} \cdot f_{x,i}. \tag{26}$$

An additional energy loss (expressed in joules) is calculated that represents resistance loss of the components of an electric drive train that is assumed to be quadratically proportional to the total propulsion force. With current I directly proportional to the wheel torque and force ($I \cong f_{xi}$), the resistive loss, P_{loss} can be calculated with a given resistance, R and the sum of the total propulsion force $\sum f_{x,i}$.

$$P_{loss} = I^2 R \cong R \cdot \sum {f_{x,i}}^2. \tag{27}$$

Resistance R is assumed to be $R = 0.001\ \Omega$, which means that the resistive power loss is very low compared to the mechanical power that will propel the vehicle. The resistive power loss has significant influence on the general driving behaviour for the vehicle in the optimisation and was arbitrarily set to limit the maximal total vehicle longitudinal acceleration. Without the resistive loss the optimal solution otherwise is to coast trough the manoeuvre and at the end apply full acceleration to reach the required exit speed. Adding the power loss forces the solution to keep a more even vehicle speed. Finally, the cost function, i.e. the calculated energy consumption, is then defined as:

$$J = \int_{t=0}^{t_{final}} (P_1 + P_2 + P_3 + P_4 + P_{loss}) dt. \tag{28}$$

The resistive power loss together with the assumption of no addition of rolling resistance or aerodynamic drag in the model (since the manoeuvre is assumed to be run with almost constant speed and therefore constant aerodynamic drag and rolling loss), results in less variation of vehicle speed. Otherwise the optimisation tends to produce solutions that have very uneven speed, resulting in no propulsion through the manoeuvre, and then saturation of the propelling force to finally reach the set exit speed, which would be uncomfortable for the passengers. To be able to study the effects of individual wheel control, the force that reduces the velocity is the cornering resistance.

5. OPTIMISATION RESULTS

Figure 5 shows the accumulated cost through the manoeuvre for the vehicle configurations studied. The vehicle which was found to consume least energy through the manoeuvre is *Vehicle F* with full individual steering and drive. Most energy is consumed by *Vehicle A* with only front axle steering and equal propulsion of all four wheels. This vehicle is the reference when comparing the energy consumption. The largest improvement achieved is by adding rear axle steering, as can be seen from Figure 5. Individual propulsion gives slightly better performance between two vehicles with the same steering configuration. In Table 5 the total energy consumption and the difference relative to the highest energy consumption for all vehicle configurations are shown.

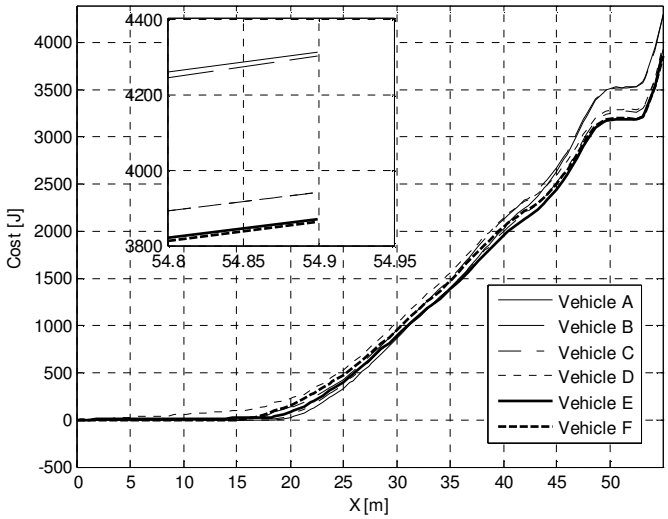

Figure 5. Cost as a function of longitudinal position through the manoeuvre for the different vehicle configurations including a magnification of the final total energy consumed.

Table 5. Consumed energy (i.e. cost) for all vehicle configurations in the optimisation study.

Vehicle configuration	Actuator configuration	Consumed energy [J]	Difference relative to highest consumed energy [%]
A	FAS + 4WD	4312.4	0
B	FAS + i-AWD	4302.7	-0.2
C	FAS + RAS + 4WD	3940.3	-8.6
D	FAS + RAS + i-AWD	3939.8	-8.6
E	AWS + 4WD	3868.7	-10.3
F	AWS + i-AWD	3861.9	-10.4

Conservation of energy for the vehicle is directly proportional to conservation of speed. Adding rear axle steering enables less energy to be consumed on actuation of the vehicle's yaw motion. Figure 6 shows the yaw rate for the vehicle configurations. Note that vehicles C-F all follow a similar trajectory and are therefore bundeled together. The vehicles with AWS give the lowest yaw rate through the manoeuvre. Studying the slip angle in Figure 6, the vehicles with AWS show very large body slip angle early in the manoeuvre. This is because the solution wants to begin the lateral movement of the chassis as soon as possible. With AWS, it can begin to build up lateral force on all wheels compared to the FWS vehicle that first needs to rotate the chassis for the rear wheels to begin producing lateral force.

A comparison between *Vehicles A, D* and *F* can be seen in Figure 7. The largest difference is at the beginning of the manoeuvre as *Vehicles D* and *F* begin to steer all wheels to move the vehicle sideways (Figure 7 (a-b)). Not that the left right steering angle difference is only visible for vehicle F with individual steering. Vehicle D has smaller difference between left and right steering angle resulting in the lines merging. In Figure 7 (c), the path is almost identical for all vehicles. Cones and boundaries around critical cones according to Equation 23 are also plotted in Figure 7 (c). When studying the lateral acceleration and yaw acceleration (Figure 7 (d-e)), it can be seen that yaw acceleration through the manoeuvre is much lower. At the beginning, the initial peak in yaw acceleration is much lower for *Vehicle F*. Instead, the lateral acceleration is higher, i.e. excitation of yaw motion is minimised, which requires less energy to follow the trajectory.

The longitudinal drive forces and friction utilisation of *Vehicles A* and *F* are shown in Figure 8. For *Vehicle F*, the optimisation solution chooses to put drive forces on the outer front wheel. No force is used on the rear wheels. Studying the friction utilisation in Figure 8, it can be seen that the rear wheels, due to rear axle steering, give initially higher friction utilisation for *Vehicle F* compared to *Vehicle A*. However, the maximum friction utilisation is reduced slightly for all wheels.

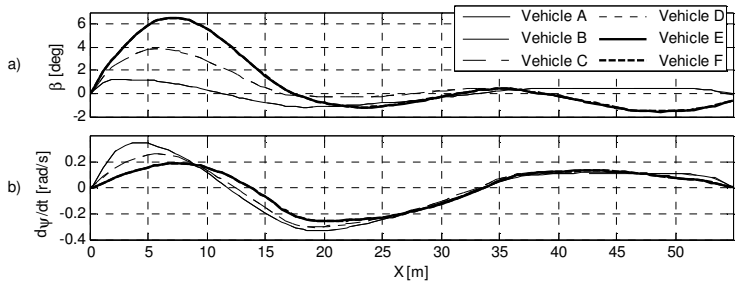

Figure 6. (a) Vehicle body slip angle and (b) yaw rate as functions of longitudinal position for the different vehicle configurations. Note that vehicles with similar steering are bundled together: (A with B), (C with D) and (E with F).

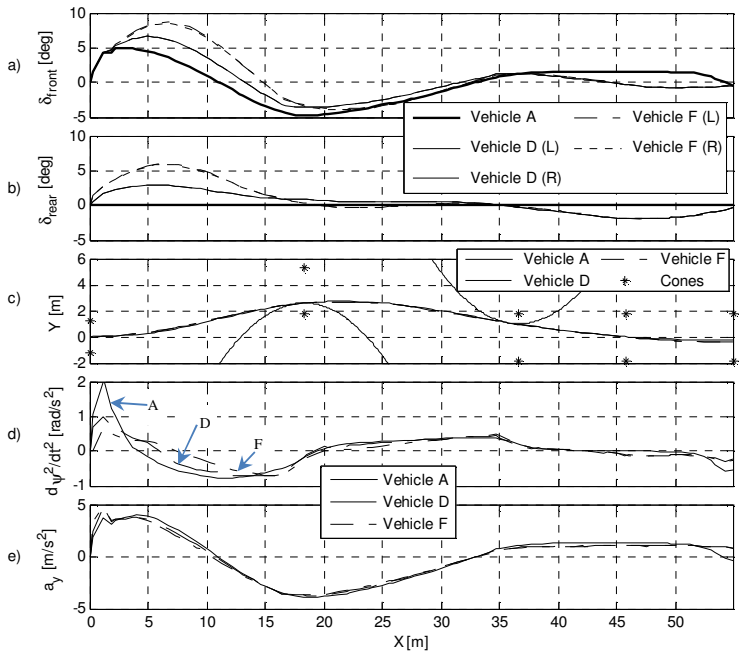

Figure 7. (a) Front and (b) rear steering angles, (c) vehicle paths, (d) yaw acceleration and (e) lateral acceleration of *Vehicles A*, *D* and *F* as functions of longitudinal position. Note that the front and left steering angles for *Vehicle D* are identical and for *Vehicle F* they are almost identical.

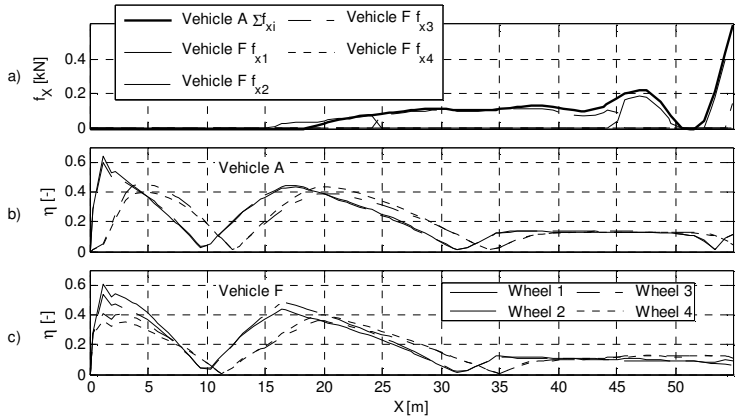

Figure 8. (a) Total longitudinal propulsion force of *Vehicle A* and individual propulsion forces of *Vehicle F*, (b) friction utilisation of *Vehicle A* and (c) friction utilisation of *Vehicle F* as functions of longitudinal position.

From the optimisation results, the two main types of behaviour that result in less energy being consumed are summarised as:

- Drive on outer front wheel for maximum contribution of yaw torque (i.e. Torque Vectoring Control)
- Limit yaw acceleration and yaw rate with rear axle steering (i.e. Rear Axle Steering)

6. SIMULATION OF CONTROL STRATEGIES

Based on the findings from the optimisation study, simplified algorithms to control wheel steering angles and propulsion torques that are more energy-efficient compared to a standard vehicle configuration are proposed. To be able to evaluate the proposed control algorithms, a whole system model is needed, including vehicle, driver and a desired path for the driver to follow. Figure 9 shows all the parts needed to model the system.

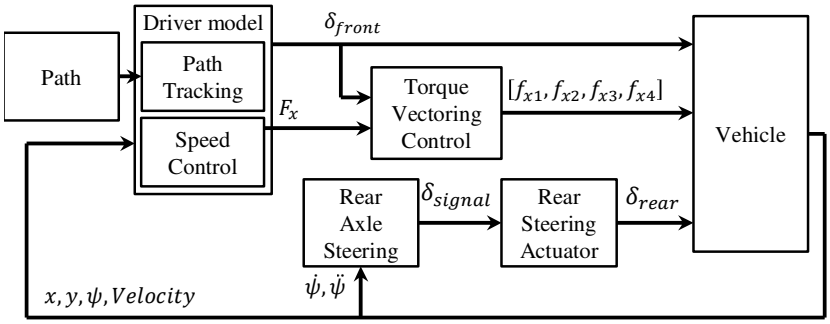

Figure 9. Block diagram of the simulation study, including vehicle, driver, desired path and control algorithms.

6.1 Driver model

To be able to evaluate control strategies by simulation, a driver model is needed. The driver's task is to follow a given trajectory at a given speed. The path tracking model and speed control model are described below.

6.1.1 Path tracking

This part of the driver model is here chosen to be a simple path tracking algorithm that has as input the desired path. The desired path is made to follow the numerical solution from the optimisation study and is given as a set of analytical equations in order to have a smooth continuous input for the simulation study.

$$y_{path} = \begin{cases} 0 & x \leq 0.5 \\ -\cos\left(\frac{(x-0.5)\cdot\pi}{21}\right)\cdot 2.75 & 0.5 < x \leq 21.5 \\ \cos\left(\left(\frac{x-21.5}{32.5}\right)^{0.9}\cdot\left(1+0.1\sin\left(\left(\frac{x-21.5}{32.5}\right)\cdot\pi\right)\right)\cdot\pi\right)\cdot 1.475 + 1.275 & 21.5 < x \leq 54 \\ -0.2 & 54 \leq x \end{cases} \quad (29)$$

In Figure 10, the path according to Equation 29 is shown together with the path from the optimisation study presented in Chapter 5. Instead of using the discrete path given by the optimisation, an analytical expression is used. The path-tracking algorithm steers the front wheels of the vehicle at the same steering angle.

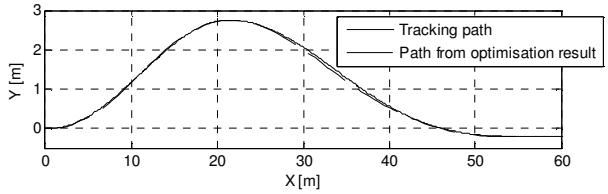

Figure 10. Given path $f(x)$ tracked by the driver model and path from optimisation study. Maximum off-tracking distance is 0.08 m.

From a given input vehicle position, a point on the path in front of the vehicle is given by the path function.

$$y_{path} = f(x + x_{preview}) \quad (30)$$

where $x_{preview}$ is a preview distance that is a tuneable parameter of the driver model, see Figure 11. The lateral distance Δy between the chassis and the preview point is calculated as:

$$\Delta y = y - y_{path}. \quad (31)$$

The angle α between the chassis and preview point is then:

$$\alpha = \tan^{-1}\frac{\Delta y}{x_{preview}}. \quad (32)$$

Finally, the steering angle δ is calculated:

$$\delta = -k_{driver}(\psi + \alpha). \quad (33)$$

where k_{driver} is a tuneable gain factor.

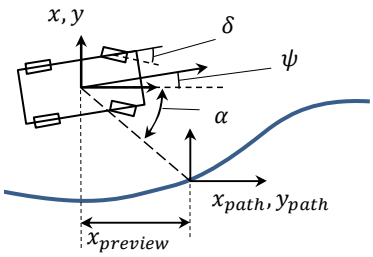

Figure 11. Driver model parameters.

The driver parameters are here set to $k_{driver} = 17$ and $x_{preview} = f$, resulting in a placement of the preview point directly on the front axle with a high gain that follows the path.

6.1.2 Speed control

A simple P speed controller is included in the driver model in order to be able to get the same exit speed as the entry speed. Since rolling resistance and aerodynamic drag are ignored, there is no need for an integrating part of the speed control. The total velocity v_{tot} of the vehicle is:

$$v_{tot} = \sqrt{{v_x}^2 + {v_y}^2} \quad (34)$$

and with the set speed (v_{set} = 12 m/s) and the proportional constant (k_p = 4000) the total propulsion force F_p is calculated as:

$$F_p = (v_{set} - v_{tot}) \cdot k_p \quad (35)$$

6.2 Torque vectoring control

As observed in the optimisation study, the solution for torque distribution between the wheels showed that it was preferable during cornering to drive on only the outer front wheel. In the manoeuvre, the yaw torque is mainly given by lateral forces but longitudinal tyre forces also contribute. The only forces that ultimately slow the vehicle down and therefore require more energy input are the cornering resistance due to lateral forces and wheel steering angles. So if less lateral forces are needed to yaw the vehicle, the less energy is wasted. If propulsion forces are used to give extra yaw torque, the outer wheels are preferable. The front outer wheel is also always steering into the direction of the corner and the resulting propulsion on that wheel will give the biggest yaw torque and some extra lateral force into the corner.

The distribution of wheel torques is made in five different variants in order to evaluate drive trains found in today's vehicles compared to the proposed torque distribution algorithms. The first three control strategies represent four wheel drive with static equal distribution of wheel force on all four wheels (*Vehicle G*), front wheel drive with equal distribution (*Vehicle H*) and rear wheel drive (*Vehicle I*). *Vehicles J* and *K* are equipped with simplified and advanced torque vectoring, respectively. The torque vectoring strategies and rear axle steering strategy are introduced in the following paragraphs.

6.2.1 Simplified torque vectoring

The fourth control strategy (*Vehicle J*) is only driving on the outer front wheel, just as observed in the optimisation study. The ratio between the front wheels is given by the steering angle rate which indicates the direction that the driver wishes to turn. From the optimisation results it was found that torque vectoring has a strong correlation to the derivative of the steering angle, which can be explained by the steering rate that gives yaw acceleration, which in turn requires yaw torque. The left and right front driving ratios κ_{FL} and κ_{FR} are given by:

$$\kappa_{FL} = 0.5 \cdot \left(\tanh\left(\dot{\delta} \cdot k_r\right) + 1\right) \quad (36)$$

$$\kappa_{FR} = 0.5 \cdot \left(-\tanh\left(\dot{\delta} \cdot k_r\right) + 1\right) \quad (37)$$

where $\dot{\delta}$ (the steering angle rate) is given by the driver and the value of k_r can be adjusted to give a more or less smooth transition of torque between the front wheels. The parameter $k_r = 0.1$ has been selected in this work to

get a smooth transition. Figure 12 shows the ratio of normalised wheel torque between the front wheels as a function of the steering angle rate.

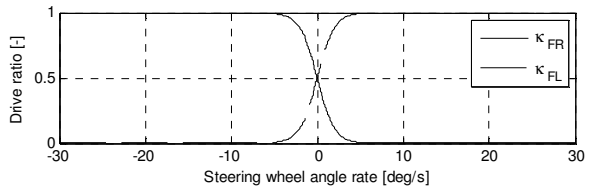

Figure 12. Drive ratio as a function of steering angle for the simplified torque vectoring strategy.

Table 6 show all the studied control strategies, where the actual force sent to an individual wheel is:

$$f_{xi} = F_p \cdot \kappa_i \tag{38}$$

Where F_p is the requested vehicle propulsion force and κ_i as $i \in \{1,2,3,4\} = \{FL, FR, RL, RR\}$.

Table 6. Torque distribution settings in the five studied control strategies.

Vehicle	Setting	κ_{FL}	κ_{FR}	κ_{RL}	κ_{RR}
G	4WD	0.25	0.25	0.25	0.25
H	FWD	0.5	0.5	0	0
I	RWD	0	0	0.5	0.5
J	s-TVC	$0.5 \cdot (\tanh(\delta \cdot k_r) + 1)$	$0.5 \cdot (-\tanh(\delta \cdot k_r) + 1)$	0	0
K	a-TVC	-	-	-	-

6.2.2 Advanced torque vectoring

Instead of using the simplified approach described in Section 6.2.1, the advanced torque vectoring algorithm described here is implemented in *Vehicle K* in order to minimise the contribution to vehicle lateral force and yaw torque produced by lateral tyre forces. This algorithm is able to put torques on all four wheels and uses vehicle states and knowledge of tyre stiffness. The advanced algorithm utilises optimisation to solve the under-determined problem of allocating the requested vehicle propulsion force F_p from the driver to the four wheel propulsion forces.

$$\min g(\boldsymbol{u}) = \min_{\boldsymbol{u}} \frac{1}{2} (\|\mathbf{WA}\boldsymbol{y} - \mathbf{WB}\boldsymbol{u}\|_2^2) \tag{39}$$

subject to u ≥ 0 and $\sum_{\mathbf{1}}^{\mathbf{4}} \boldsymbol{u} = F_p$.

$\boldsymbol{u} = [f_{x1}\ f_{x2}\ f_{x3}\ f_{x4}]^{\mathrm{T}}$ represents the longitudinal tyre forces and $\boldsymbol{y} = \left[-C_f\alpha_1\ -C_f\alpha_2\ -C_r\alpha_3\ -C_r\alpha_4\right]^{\mathrm{T}}$ the lateral forces given by the slip angles and tyre stiffness C_f and C_r given by:

$$C_f = B_1 \cdot \frac{b}{f+b} \cdot m \cdot g \tag{40}$$

$$C_r = B_3 \cdot \frac{f}{f+b} \cdot m \cdot g \tag{41}$$

The slip angles α_{1-4} are calculated from vehicle states v_x, v_y and $\dot{\psi}$.

$$\begin{aligned} \alpha_1 &= \tan^{-1}\left(\frac{v_y + f\dot{\psi}}{v_x - \frac{wb}{2}\dot{\psi}}\right) - \delta_1, \quad \alpha_2 = \tan^{-1}\left(\frac{v_y + f\dot{\psi}}{v_x + \frac{wb}{2}\dot{\psi}}\right) - \delta_2 \\ \alpha_3 &= \tan^{-1}\left(\frac{v_y - b\dot{\psi}}{v_x - \frac{wb}{2}\dot{\psi}}\right) - \delta_3, \quad \alpha_4 = \tan^{-1}\left(\frac{v_y - b\dot{\psi}}{v_x + \frac{wb}{2}\dot{\psi}}\right) - \delta_4 \end{aligned} \tag{42}$$

A and **B** are the geometry matrices, composed of the vehicle track width, front and rear axle distance to the centre of gravity and the steering angles. These matrices calculate the contribution to vehicle lateral force and yaw moment from tyre lateral forces $\boldsymbol{y}$ and longitudinal forces $\boldsymbol{u}$.

$$\mathbf{A} = \begin{bmatrix} \cos\delta_1 & \cos\delta_2 & \cos\delta_3 & \cos\delta_4 \\ \left(\frac{-wb}{2}\sin\delta_1 + f\cos\delta_1\right) & \left(\frac{wb}{2}\sin\delta_2 + f\cos\delta_2\right) & \left(\frac{-wb}{2}\sin\delta_3 - b\cos\delta_3\right) & \left(\frac{wb}{2}\sin\delta_4 - b\cos\delta_4\right) \end{bmatrix} \quad (43)$$

$$\mathbf{B} = \begin{bmatrix} \sin\delta_1 & \sin\delta_2 & \sin\delta_3 & \sin\delta_4 \\ \left(\frac{-wb}{2}\cos\delta_1 + f\sin\delta_1\right) & \left(\frac{wb}{2}\cos\delta_2 + f\sin\delta_2\right) & \left(\frac{-wb}{2}\cos\delta_3 - b\sin\delta_3\right) & \left(\frac{wb}{2}\cos\delta_4 - b\sin\delta_4\right) \end{bmatrix} \quad (44)$$

$\mathbf{W} = \begin{bmatrix} w_1 & 0 \\ 0 & w_2 \end{bmatrix}$ is the weight matrix. In this case, the weight matrix is chosen to be $\mathbf{W} = \begin{bmatrix} 100 & 0 \\ 0 & 1 \end{bmatrix}$, with the highest weight for the lateral force. The algorithm calculates cost as an estimate of the total lateral force and yaw torque given from the lateral tyre forces and then subtracts the lateral force and yaw torque given from the longitudinal forces. To minimise the cost, the solution tries to maximise the contribution from longitudinal forces. This will give an increase in lateral force and yaw torque to the vehicle without an increase in lateral tyre forces and thus slightly less lateral force is required to follow the path. Since lateral forces alone influences the cornering resistance that slows the vehicle down, meaning that if less lateral force due to lateral slip is used, less energy is wasted at that moment in time. This optimisation problem is solved using the optimisation toolbox in Matlab [13].

6.3 Rear axle steering

As can be seen from the results from the optimisation study, the yaw acceleration is limited when all wheels are steered. Instead, lateral acceleration increases during those moments when yaw acceleration is limited. The rear axle steering algorithm (RAS) in this study (*Vehicle L*) is therefore constructed as a feedback controller of the yaw acceleration and yaw rate over a given threshold of yaw acceleration and rate. Equation 45 and 46 should be considered as a first attempt of a controller designed to capture this behaviour. The control signal is calculated as a continuous function of yaw acceleration:

$$\delta_{acc}^{sig} = \left(|\ddot{\psi}| - \ddot{\psi}_{th}\right) \cdot \tanh\left(\ddot{\psi} \cdot 100\right) \cdot K_{acc} \cdot \left(\tanh\left(\left(|\ddot{\psi}| - \ddot{\psi}_{th}\right) \cdot 500\right) + 1\right) \cdot 0.5. \quad (45)$$

and for yaw rate as:

$$\delta_{rate}^{sig} = \left(|\dot{\psi}| - \dot{\psi}_{th}\right) \cdot \tanh\left(\dot{\psi} \cdot 100\right) \cdot K_{rate} \cdot \left(\tanh\left(\left(|\dot{\psi}| - \dot{\psi}_{th}\right) \cdot 500\right) + 1\right) \cdot 0.5. \quad (46)$$

The total signal is combined:

$$\delta_{rear}^{sig} = \delta_{acc}^{sig} + \delta_{rate}^{sig} \quad (47)$$

where $\ddot{\psi}_{th} = 0.5\ rad/s^2$ and $\dot{\psi}_{th} = 0.1\ rad/s$ are the threshold values above which rear axle steering is activated and $K_{acc} = 0.1$ and $K_{rate} = 0.3$ are the gains in the amount of steering above the threshold. Figure 13 shows the resulting signal as a function of yaw acceleration and yaw rate.

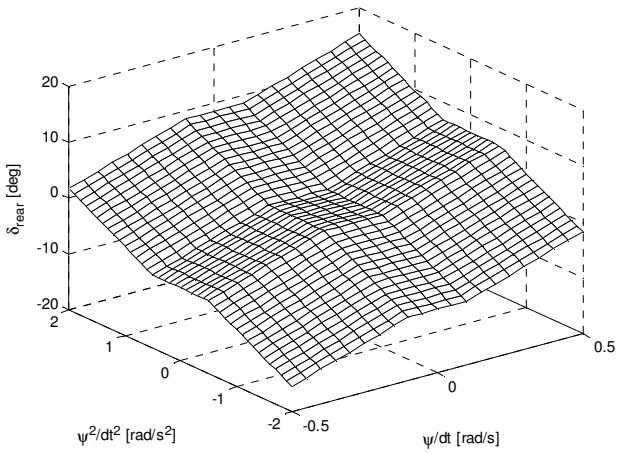

Figure 13. Illustration of the characteristics of the *RAS* function described in equations 45-47 i.e. the resulting rear axle steering angle signal as function of yaw acceleration and yaw rate for *Vehicle L*.

Vehicle M, which has rear axle steering that is 50 % proportional of the front axle steering angle is also included as a reference.

6.3.1 Rear axle steering actuator

The resulting steering signal calculated by the controller is not sent directly to the rear wheels but to a rear wheel steering actuator that is physically modelled with maximum rate, maximum angle and relaxation dynamics. The reason is both to handle numerical issues and to have a reasonable dynamic response of an electrically controlled actuator. The actuator chosen for the presented study has a maximum rate of 5 deg/s and a response time of 0.05 s.

7. SIMULATION RESULTS

The resulting energy consumption calculated by simulation for the vehicles with different control strategies (*Vehicles G* to *M*) is shown in Figure 14 and Table 7. The energy consumption is calculated in the same way as in the optimisation study using Equations 26-28 and *Vehicle G* is selected as the reference for the energy comparison.

Most energy consumed is by *Vehicle I*, which is a configuration with RWD and FAS. The front wheel drive vehicle is better and in-between them comes the four wheel drive vehicle (4WD). The two different torque vectoring controls (*Vehicles J* and *K*) show further improvement and almost similar total energy consumption. Adding rear axle steering (*Vehicles L* and *M*) reduces energy consumption even further. The largest difference is found between *Vehicle I* and *M* (vehicle with both TVC and 50 % proportional RAS), where *Vehicle M* consumes about 8 % less cornering energy.

Table 7. Consumed energy (i.e. cost) for all vehicles with different control strategies in the simulation study for the chosen manoeuvre.

Vehicle Configuration	Control strategy	Consumed energy /cost [J]	Difference relative to highest consumed energy [%]
G	4WD	4676.0	0
H	FWD	4665.4	-0.2
I	RWD	4682.2	0.1
J	s-TVC	4630.7	-1.0
K	a-TVC	4630.8	-1.0
L	s-TVC + RAS	4403.4	-5.8
M	s-TVC + (RAS = 50% FAS)	4284.6	-8.4

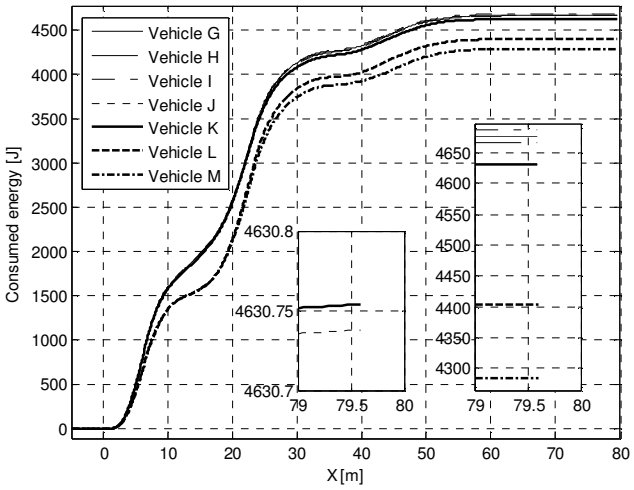

Figure 14. Simulated energy consumed through the manoeuvre for all vehicles with different control strategies as a function of longitudinal position including magnifications of the final total energy consumed.

Figure 15 shows a comparison of the propulsion forces. The simplified torque vectoring control algorithm (*Vehicle J*) only drives on the front wheels and shifts which side it drives on as a function of the steering wheel rate. The advanced torque vectoring control algorithm (*Vehicle K*) finds almost the same solution, where the outer wheel is

driven. It is also seen that propulsion force converges to zero at the end of the manoeuvre when the vehicle reaches the set speed.

In Figure 16 (a-b) the vehicle body side slip and yaw rate is shown for *Vehicles G*, *L* and *M*. The yaw rate is kept much lower due to the rear axle steering that limits the yaw rate. There is, however, a difference between *Vehicles L* and *M* towards the end of the manoeuvre, where the proposed rear axle steering algorithm (*Vehicle L*) has less side slip.

When comparing *Vehicle G* with *Vehicles L* and *M*, it can be seen that yaw acceleration is also limited (Figure 16 (c-d)). However, maximum lateral acceleration is also somewhat limited but when RAS is active to limit yaw acceleration, the gradient of lateral acceleration increases. The difference in steering angle is shown in Figure 16 (e-f). It is shown that the driver has to steer more when RAS is activated compared to the vehicle with only front axle steering. It can also be seen that *Vehicle L* uses less steering towards the end of the manoeuvre.

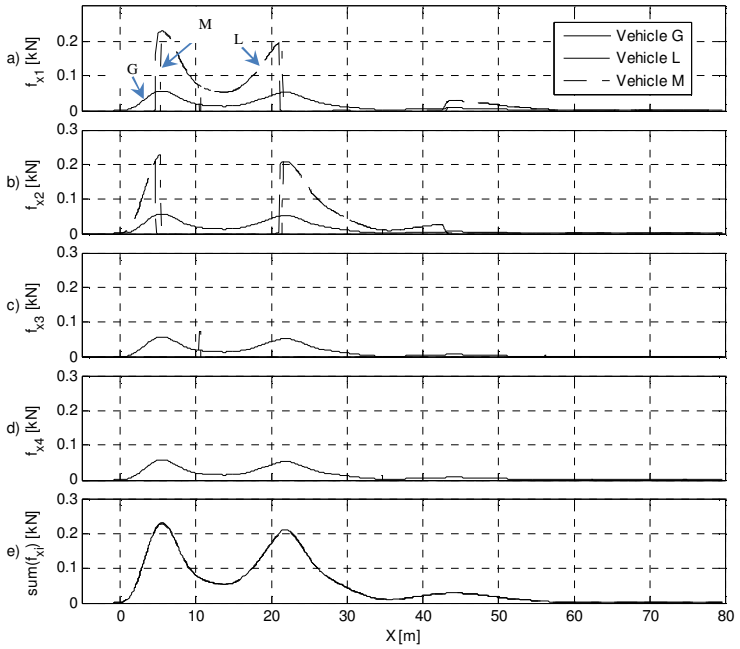

Figure 15. (a-d) Individual and (e) total propulsion forces for *Vehicles G*, *J* and *K* as a function of longitudinal position.

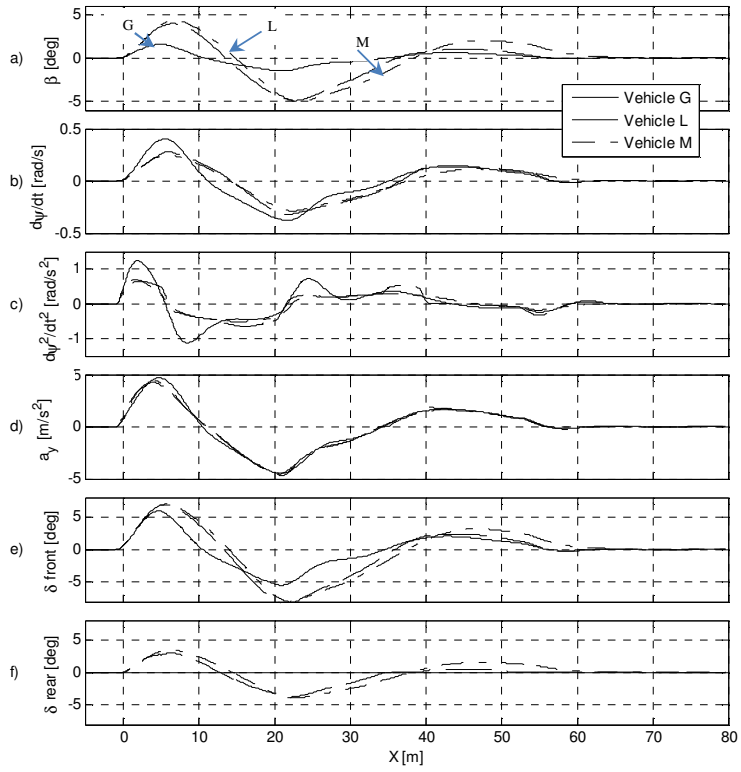

Figure 16. (a) Vehicle side slip, (b) yaw rate, (c) yaw acceleration, (d) lateral acceleration, (e) front and (f) rear steering angles of *Vehicles G*, *L* and *M*, as functions of longitudinal position.

The paths of *Vehicles G*, *L* and *M* in comparison to the desired path are shown in Figure 17 a). The driver model follows the path really well. Small differences in heading angle can be seen where the vehicle with RAS is slower to respond in yaw due to the limiting controllers.

Friction utilisation for *Vehicles G*, *L* and *M* is shown in Figure 17 (b - d). It is shown that the rear wheels, due to rear axle steering, initially have higher friction utilisation while the maximum level is lower.

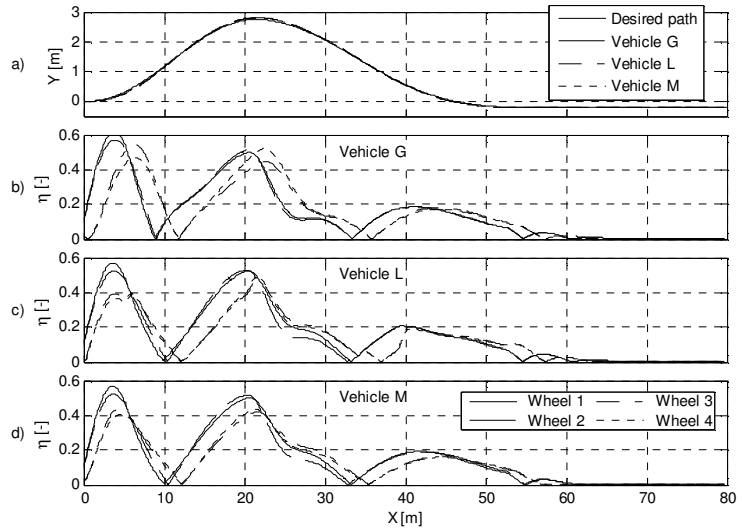

Figure 17. (a) Vehicle paths and friction utilisation for *Vehicles G* (b), *L* (c) and *M* (d) as functions of longitudinal position for the four different wheels respectively.

8. CONCLUSIONS

The aim of the work was to study how active steering and propulsion on individual wheels can be utilised in order to improve a vehicle's cornering efficiency during a double lane change manoeuvre at moderate speeds. The results show that rear axle steering can be used to limit yaw-acceleration and yaw-rate but still manage the manoeuvre. Individual propulsion torque shows that front wheel drive with torque vectoring has the highest energy efficiency. For the studied manoeuvre, the energy consumed can be reduced up to 10 % using optimal control of RAS and individual wheel torques, over the standard vehicle with only FAS and 4WD, see Table 5. Note that the improvement is valid without rolling resistance and air drag. If those losses also are taking into account, the improvement is scaled down approximately four times. However, the order of the most energy efficient vehicle persists. To be able to maximise the energy efficiency of a vehicle driving in the studied cornering case, it is found that the largest gain is obtained by introducing rear axle steering, RAS. The results show that even with limited rear axle steering performance, substantial improvement is achieved. Individual propulsion that enables torque vectoring also gives better energy efficiency, but not as much as RAS.

It is shown that front wheel drive is the most energy-efficient option especially if the torque balance can be shifted to the outer wheel. This gives both higher yaw torque and lateral force, which results in lower lateral tyre forces and slip angles. Comparison between s-TVC and a-TVC shows similar results as regards to torque distribution (Figure 18) and the resulting energy consumption (Figure 17). The close similarity of the two algorithms might be explained by that the actual optimal point when to switch the propulsion from left to right (and vice versa) is closely connected by the steering rate direction, thus resulting in very similar behaviour and final result. If wheel motor efficiency is considered as in [2] and [3], the optimal wheel torque distribution might be different. However considering that the typical efficiency of an electric motor at low torque is very low and increasing as torque is increased [14], will still indicate that it is preferable to only use only one motor at lower torque levels, instead of equally distributing a low torque on all wheel motors.

Control algorithms to control wheel torques and rear axle steering are proposed in order to mimic the behaviour from the optimisation study. When evaluating these algorithms (that are based on RAS and TVC), a combined efficiency improvement of 5-8 % is achieved for the studied vehicle model including a basic driver model following a path. Comparing the results from the optimisation study with the simulation study of the different control strategies, it is seen that distribution of propulsion force over time is different. This is due to the fact that the optimisation also finds global optima of driver signals over the whole manoeuvre, which the driver model in the simulation study is not able to .

The behaviour of individual wheel control should naturally be different in situations where the vehicle gets into at-the-limit conditions. Evenly distributing forces is less efficient from an energy efficiency point of view but

when higher acceleration levels are reached, the behaviour of the control algorithms might have to be changed to improve safety and stability.

The results in this study are based on the results from numerical optimisation. Although improvements in performance are shown, the optimisation problem is very complex and might not have found the global optimum. The control strategies from the optimisation results should be considered as *one* way to improve the energy efficiency. There is however no guarantee that the resulted optimisation solution is the one with the lowest energy consumption.

The findings from this work show that active steering and torque control can be used to reduce energy consumption. The results indicate that in order to improve energy efficiency for a vehicle driving in a non-safety-critical situation, the force distribution should be shifted towards the front wheels. These results are relevant for regular driving at low acceleration levels far from at-the-limit conditions. This is the situation most of the time during highway driving and is therefore important for reducing fuel consumption in general.

ACKNOWLEDGEMENTS

The financial support from SHC (the Swedish Hybrid and electric vehicle Centre) and TRENoP is gratefully acknowledged.

REFERENCES

[1] H. Liu, X. Chen and X. Wang, ”Overview and prospects on distributed drive electric vehicles and its energy saving strategy”, PRZEGLĄD ELEKTROTECHNICZNY (Electrical Review), ISSN 0033-2097, R. 88 NR 7a/2012, pp. 122-125, 2012.

[2] Y. Chen and J. Wang, “Energy-efficient control allocation with applications on planar motion control of electric ground vehicles”, 2011 American Control Conference, San Francisco, CA, USA June 29 - July 01, 2011.

[3] Y. Chen and J. Wang, “Adaptive energy-efficient control allocation for planar motion control of over-actuated electric ground vehicles”, IEEE transactions on control systems technology, Vol. 22, No. 4, pp. 1362-1373, 2014.

[4] Y. Suzuki, Y. Kano and M. Abe, “A study on force distribution control for full drive-by-wire electric vehicle”, Vehicle System Dynamics – International Journal of Vehicle Mechanics and Mobility, Vol. 52, pp. 235-250, 2014.

[5] A. M. Dizqah, B. Lenzo, A. Sorniotti, P. Gruber, S. Fallah, J. De Smet, “A fast and parametric torque distribution strategy for four-wheel-drive energy-efficient electric vehicles”, IEEE Transaction on Industrial Electronics, Vol. 63, No. 7, pp. 4367-4376, 2016.

[6] M. Čorić, J. Deur, J. Kasać, H.E. Tseng, D. Hrovat, ”Optimisation of active suspension control inputs for improved vehicle handling performance”, Vehicle System Dynamics – International Journal of Vehicle Mechanics and Mobility, Vol. 54, No. 11, pp.1574-1600, 2016.

[7] J. Edrén, P. Sundström, M. Jonasson, B. Jacobson, J. Andreasson and A. S. Trigell, “Road friction effect on the optimal vehicle control strategy in two critical manoeuvres”, International Journal of Vehicle Safety, Vol. 7, No. 2, pp. 107-130, 2014.

[8] H.B. Pacejka, "Tyre and vehicle dynamics", Buttherworth-Heinemann, 2005.

[9] http://www.consumerunion.org/ accessed in October 2011.

[10] J. Åkesson, K.-E. Årzén, M. Gäfvert, T. Bergdahl, and H. Tummescheit., "Modeling and optimization with Optimica and JModelica.org – languages and tools for solving large-scale dynamic optimization problems", Computers and Chemical Engineering, Vol. 34, No. 11, pp. 1737-1749, 2010.

[11] Modelica, http://www.modelica.org/ accessed in October 2013.

[12] JModelica, http://www.jmodelica.org/ accessed in October 2013.

[13] Matlab® and Simulink® (2013) The MathsWorks, Inc., Natick, Ma, USA http://www.mathworks.com, accessed in June 2014.

[14] L. C. Silva, “Modeling and design of the electric drivetrain for the 2013 research concept vehicle”, Master Thesis, XR-EE-E2C 2013:008, KTH Royal Institute of Technology, Stockholm, Sweden, 2013.